



HAL
open science

3D Ultrasound Elastography for Early Detection of Lesions. Evaluation on a Pressure Ulcer Mimicking Phantom.

Jean-François Deprez, Guy Cloutier, Cedric Schmitt, Claudine Gehin, André Dittmar, Olivier Basset, Elisabeth Brusseau

► **To cite this version:**

Jean-François Deprez, Guy Cloutier, Cedric Schmitt, Claudine Gehin, André Dittmar, et al.. 3D Ultrasound Elastography for Early Detection of Lesions. Evaluation on a Pressure Ulcer Mimicking Phantom.. Conference proceedings: .. Annual International Conference of the IEEE Engineering in Medicine and Biology Society. IEEE Engineering in Medicine and Biology Society. Annual Conference, 2007, 1, pp.79-82. 10.1109/IEMBS.2007.4352227 . inserm-00192829

HAL Id: inserm-00192829

<https://inserm.hal.science/inserm-00192829>

Submitted on 29 Nov 2007

HAL is a multi-disciplinary open access archive for the deposit and dissemination of scientific research documents, whether they are published or not. The documents may come from teaching and research institutions in France or abroad, or from public or private research centers.

L'archive ouverte pluridisciplinaire **HAL**, est destinée au dépôt et à la diffusion de documents scientifiques de niveau recherche, publiés ou non, émanant des établissements d'enseignement et de recherche français ou étrangers, des laboratoires publics ou privés.

3D Ultrasound Elastography for Early Detection of Lesions. Evaluation on a Pressure Ulcer Mimicking Phantom.

Jean-François Deprez, Guy Cloutier, Cédric Schmitt,
Claudine Gehin, André Dittmar, Olivier Basset and Elisabeth Brusseau

Abstract— A pressure ulcer is a damaged tissue area induced by an unrelieved pressure compressing the tissue during a prolonged period of immobility. The lack of information and studies on the development of this pathology makes its prevention difficult. However, it is both acknowledged that lesions initiate in the deep muscular tissues before they expand to the skin, and that lesions are harder than healthy tissues. Elastography is therefore an interesting tool for an early detection of the pathology. A 3D strain estimation algorithm is presented and evaluated on a PVA-cryogel phantom, mimicking a pressure ulcer at an early stage.

I. INTRODUCTION

Pressure ulcers, also known as bedsores, are lesions of the skin and underlying tissues, caused by a high and prolonged pressure at the body interface. This pathology concerns any people with weakened sensitivity or limited mobility. But it mostly strikes elders and spinal cord injury patients. This disease is painful, handicapping and becomes a growing issue, as life expectancy increases in western countries. Yet, it has been neglected till now, and there is still little consensus about the pathological process that triggers the formation of bedsores.

It is now acknowledged that pressure ulcers appear after a prolonged period of immobility, during which the body interface lying on a support (either a bed or a wheelchair) undergoes a high and unrelieved pressure. During a short time, biological soft tissues can tolerate relatively high pressures. However, a weaker but continuous pressure can result in severe injuries and a pressure ulcer can therefore appear anywhere in the body as soon as it is subjected to a significant pressure. Nevertheless, thin layered tissues in regard to a bony prominence are privileged regions, as a high stress is focused on a small volume. This pattern is met for sacrum or heels. These are privileged regions and 80 %

of bedsores affect these two locations.

Above a threshold, compression results in local occlusions of blood capillaries. This shortage of blood supply, called ischemia, prevents the natural exchanges of oxygen and nutrients between the blood and body cells to occur. These ischemic conditions may lead to cell death and severe tissue damages. Besides, skin and muscle have different metabolisms: skin metabolism is anaerobic, while muscle has an aerobic metabolism, requiring much more oxygen [1]. Muscles are therefore more vulnerable to ischemia than the skin and surrounding fat tissues. Thus, lesions first initiate in the deep muscle tissue before expanding to the skin, making difficult their early detection. This explains why the sore is already at a severe stage when it appears on the skin surface.

In the literature, few studies are available on pressure ulcer mechanical properties. The main reference in this area is given by Gefen *et al.* [2], who showed that tissues damaged by pressure ulcer are harder than healthy tissues. By applying a prolonged compression on rat muscle tissues *in vivo*, they observed a significant increase of tissue elastic modulus with time and pressure level.

Because of this process of hardening of damaged areas and the deep origin of the ulcer, ultrasound elastography seems especially appropriate for the early detection of pressure ulcer formation.

Elastography is a promising technique, which aim is to provide information about the mechanical properties of soft biological tissues, by investigating their deformation under an external load. Pre- and post-compression ultrasonic (US) radio-frequency (RF) signals are first acquired. Then, changes within the signals induced by the stress are analyzed to compute a map of local strains.

Since static elastography has appeared in the early 90s [3], mainly 1D methods were developed. A few 2D methods have also been worked out [4]-[10]. These techniques are adapted to current clinical equipment since ultrasound scanners essentially provides 2D data. However they may lead to noisy elastograms if significant out-of plane motion occurs, since it represents a source of decorrelation between pre- and post-compression signals. To overcome this decorrelation problem, and with the development of 2D transducer arrays, we use in this study a 3D estimator, which computes the axial strain while considering lateral and azimuthal motions. This strain estimation model is further

Manuscript received April 2, 2007. This work was supported in part by a grant of the Region Rhône-Alpes, France.

J.F. Deprez, O. Basset and E. Brusseau are with the laboratory CREATIS (Application & Research Center for Image and Signal Processing), INSA-Lyon, Université de Lyon, CNRS UMR 5220 & INSERM U630 (corresponding author mail: 7 avenue Jean Capelle, Villeurbanne, 69621 France; phone: 33 4 72 43 62 54; fax: 33 4 72 43 85 26; e-mail: deprez@creatis.insa-lyon.fr).

G. Cloutier and C. Schmitt are with the Laboratory of Biorheology and Medical Ultrasonics of the University of Montreal Hospital, Canada (e-mail: guy.cloutier@umontreal.ca, cedric.schmitt@umontreal.ca).

C. Gehin and A. Dittmar are with the Biomedical Microsensors Department of Institut des Nanotechnologies de Lyon of INSA (National Institute of Applied Sciences), France (e-mail: claudine.gehin@insa-lyon.fr and andre.dittmar@insa-lyon.fr).

This material is presented to ensure timely dissemination of scholarly and technical work.

Copyright and all rights therein are retained by authors or by other copyright holders.

All persons copying this information are expected to adhere to the terms and constraints invoked by each author's copyright. In most cases, these works may not be reposted without the explicit permission of the copyright holder.

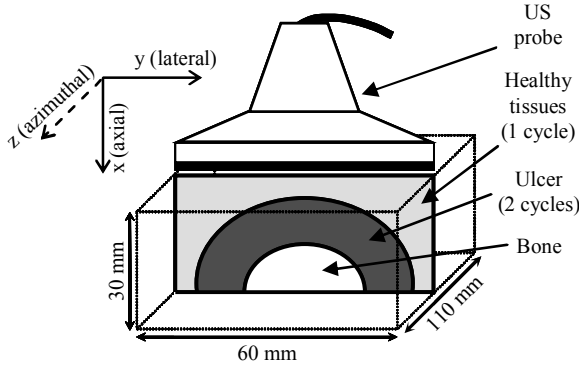


Fig. 1. Phantom scheme.

detailed in the following section. Pressure ulcer early detection is then investigated with the proposed method.

II. METHOD

The proposed 3D strain estimator is based on an adaptive and iterative constrained optimization process. For each elementary RF region R_1 selected in the pre-compression volume V_1 , its deformed version R_2 is searched in the post-compression volume V_2 and the corresponding local strain is then estimated. In the axial direction (see directions in fig. 1), R_2 is considered as a time-delayed (parameter d) and scaled (parameter α) replica of R_1 . Because lateral and azimuthal resolutions are much coarser than the axial resolution, R_2 is only considered to be a shifted version of R_1 in these directions (parameters τ and ν). The axial delay d results from the accumulation of axial deformations of the regions located between the probe and the region of interest. After having compensated for this axial delay, three parameters remain to be calculated: the axial scaling factor α , the lateral shift τ and the azimuthal shift ν . They are estimated as the arguments that minimize an objective function f , defined as the opposite of the correlation coefficient between R_1 and its deformed version R_2 compensated for the three parameters. Since this objective function f may suffer from multiple local minima, and could therefore yield to incorrect estimations, strong constraints are introduced on the different arguments. An admissible set of values is thus defined.

A three step process is applied to compute the strains. First, an adaptive windowing of the region of study is used, followed by the joint estimation of the three parameters α , τ and ν . The strain map is finally computed.

A. Adaptive windowing of the region of study

The axial tissue compression yields also to lateral and out-of-plane motion in the region of interest, resulting in a transformation of the acoustical footprint of the pre-compression signal. To overcome the subsequent loss of correlation, an adaptive displacement of the 3D region of study is considered. It allows tracking the motion of the

scatterers due to the compression and enables to work on corresponding tissue regions, and therefore equivalent US data in both volumes. To cover the whole US volume V_1 , the pre-compression region of study R_1 is regularly moved by constant steps of Δ_{ax} , Δ_{lat} , and Δ_{azim} in the axial, lateral and azimuthal directions, respectively. An adaptive displacement is considered for R_2 : its axial displacement results from the accumulation of axial deformations of the regions located between the probe and the region of interest, and the lateral and azimuthal displacements are directly linked to those estimated over adjacent regions. u_{R1} and u_{R2} , the positions of R_1 in V_1 and R_2 in V_2 , respectively, are then given by:

$$u_{R_1}(m, n, q) = m \cdot \Delta_{ax} \cdot \vec{i} + n \cdot \Delta_{lat} \cdot \vec{j} + q \cdot \Delta_{azim} \cdot \vec{k} \quad (1)$$

$$u_{R_2}(m, n, q) = \sum_{k=0}^{m-1} \left(\frac{1}{\alpha_k} \right) \cdot \Delta_{ax} \cdot \vec{i} + \sum_{k=0}^{n-1} \tau_k \cdot \vec{j} + \sum_{k=0}^{q-1} \nu_k \cdot \vec{k}$$

where α_k is the axial scaling factor at position $u_{R1}(m, n, q)$, τ_k the lateral displacement and ν_k the azimuthal displacement, estimated on step k . The axial time-delay (parameter d) is directly linked to the axial coordinate of u_{R2} . Hence, with such an initialization for the location of R_2 in V_2 , the parameter d is already determined, and the three parameters α , τ and ν remain to be estimated, the two latter being of small magnitude.

B. Joint estimation of the parameters α , τ and ν

A joint estimation of the parameters α , τ and ν is then performed. The region of interest R_2 is searched within V_2 , as an axially scaled, laterally and azimuthally shifted replica of R_1 , noted $R_2(ax, y + \tau, z + \nu)$. This is done thanks to the minimization of the objective function f , which computes the opposite of the normalized correlation coefficient between R_1 and R_2 , when R_2 is compensated for the three searched parameters:

$$[\hat{\alpha}, \hat{\tau}, \hat{\nu}] = \arg \min_{\alpha, \tau, \nu} f(\alpha, \tau, \nu), \quad (2)$$

with:

$$f(\alpha, \tau, \nu) = - \sum_{x, y, z} \tilde{R}_1(x, y, z) \cdot \tilde{R}_2(\alpha x, y + \tau, z + \nu) \quad (3)$$

$$\sqrt{\sum_{x, y, z} (\tilde{R}_1(x, y, z))^2} \cdot \sqrt{\sum_{x, y, z} (\tilde{R}_2(\alpha x, y + \tau, z + \nu))^2}$$

$$\text{where } \tilde{R}_i(x, y, z) = R_i(x, y, z) - \bar{R}_i(x, y, z). \quad (4)$$

$\bar{R}_i(x, y, z)$ is the mean value of the region R_i . In elastography, deformations are of small magnitude (a few %). The optimization is therefore submitted to a set of linear inequalities constraints, drastically limiting the occurrence of local minima:

$$\alpha_{\min} \leq \alpha \leq \alpha_{\max}, \quad \tau_{\min} \leq \tau \leq \tau_{\max}, \quad \nu_{\min} \leq \nu \leq \nu_{\max}. \quad (5)$$

Reducing the parameter domain also saves calculation time. The algorithm is implemented as a descent method, following the scheme:

$$(\alpha_{k+1} \quad \tau_{k+1} \quad \nu_{k+1}) = (\alpha_k \quad \tau_k \quad \nu_k) + \rho_k \cdot \mathbf{S}_k \quad (6)$$

where ρ_k is the descent step computed by a linear search, and S_k is the descent direction.

The first iteration is chosen as the middle of the admissible set $K = \{(\alpha, \tau, \nu) \mid \alpha_{min} \leq \alpha \leq \alpha_{max}, \tau_{min} \leq \tau \leq \tau_{max}, \nu_{min} \leq \nu \leq \nu_{max}\}$, and a sequence of admissible iterations is then generated, until a stop criteria is met.

C. Strain computation

Strain maps are then computed thanks to the set of parameters calculated for the whole US volume. We focus here on the axial strain, which is directly linked to the estimated parameter α_k according to the relation:

$$\hat{\epsilon}_{ax,k} = \frac{1}{\hat{\alpha}_k} - 1. \quad (7)$$

III. EXPERIMENTAL RESULTS

A polyvinyl alcohol (PVA) cryogel phantom was designed to mimic a pressure ulcer at an early stage. Since PVA cryogel is a material whose acoustical properties are very close to those of soft biological tissues, it can easily be imaged with an ultrasound device. Moreover its stiffness increases with the number of freeze-thaw cycles applied. This typically allows encompassing the range of elasticity values commonly met in soft biological tissues [11].

As previously mentioned, pressure ulcers are found on sites where thin layered tissues are in regard to a bony prominence. Therefore, the phantom is designed as a parallelepiped of dimensions 30 mm x 60 mm x 110 mm, with three distinct areas: a bone, a region mimicking the pressure ulcer at an early stage and healthy tissues surrounding it. The geometry is further detailed in figure 1. The bone, taken from the forward limb of a dog, measured 10 mm in diameter. The pathological area underwent 2 freeze-thaw cycles, which is one more than the healthy region. This led to a harder material for the pressure ulcer mimicking area [12].

Acquisitions of RF US data were performed with an *Ultrasonix - Sonix RP* device. The probe and sampling frequencies were 7 MHz and 40 MHz, respectively. Each image was composed of 128 RF A-lines, with a line interdistance of 0.29 mm. A linear stepper motor was used to move the probe azimuthally and to acquire regularly spaced 2D scans (by steps of 0.2 mm). A first set of scans was performed with the phantom in a pre-compression state. The corresponding RF data volume was built by stacking the images. Then a flat plate was used to uniformly compress the phantom and achieve a global axial deformation of 2%, and the same protocol was once again applied to compute the post-compression volume.

The ability of our algorithm to detect the pathological area was evaluated on these data. The size of the region of interest R_1 was 60 axial points x 3 RF lines x 3 azimuthal

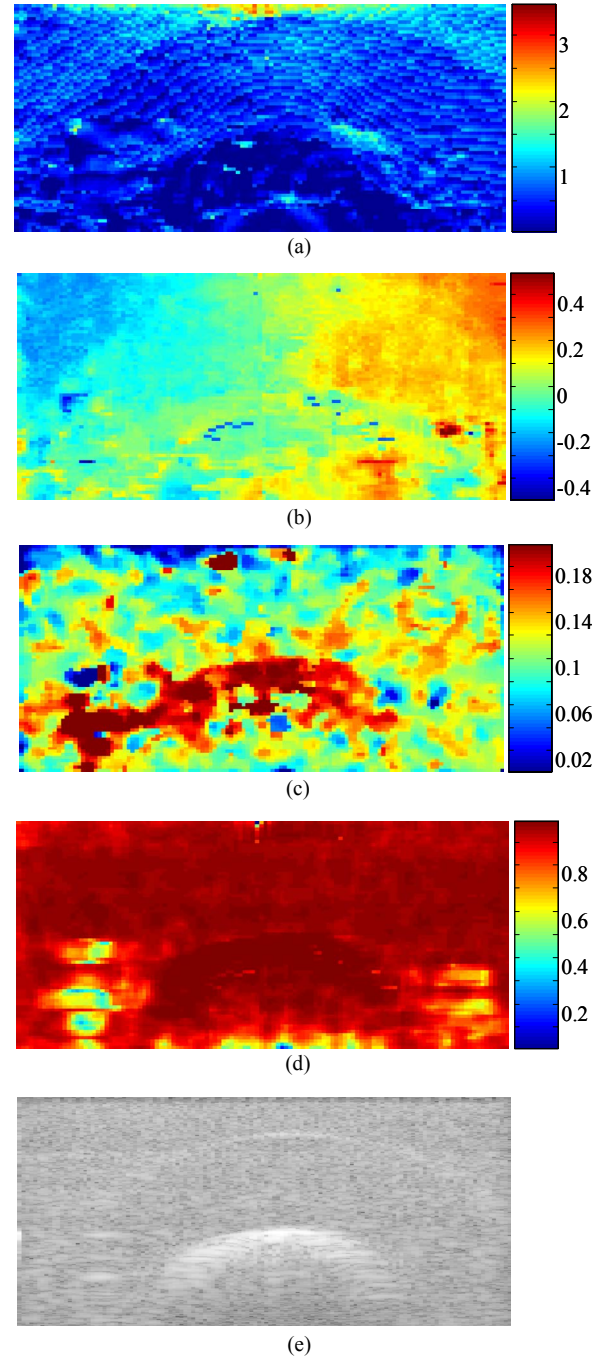


Fig. 2. Results for a volume centered on the middle of the phantom. (a) is the axial strain (%). (b) is the lateral displacement (mm). (c) is the azimuthal displacement (mm). (d) is the correlation coefficient map. (e) is a B-mode image.

slides, and the overlap was 80 %, both axially and laterally (no azimuthal overlap). The results for an area centered on the middle of the phantom are presented in fig. 2. A B-mode image of the region is shown in fig. 2e. Even if the bone is visible because of its echogenicity, the echography does not exhibit any mechanical information. On the contrary, the axial strain map (fig. 2a) is of great help for distinction between the lesion, the healthy tissues and the bone. Due to

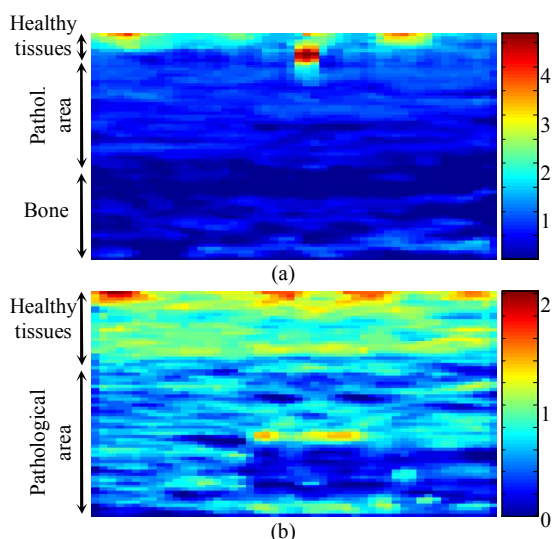


Fig. 3. Axial strain along the z axis, for a slice centered on the middle of the phantom (a), and for an off-centered slice (b).

the low compression level, strain values remain within a small range. However, the deformation of the bone is almost zero, while the mean axial strain of the pathological area is about half that of surrounding tissues (0.75% vs. 1.5%). Moreover, the boundary between the healthy region and the ulcer is recognizable, which could allow a diagnostic about the stage of the illness. The lateral displacement map (fig. 2b) displays this limit too, especially in the top corners of the image. Azimuthal displacement estimations are shown fig. 2c. Surprisingly, there are large displacements for tissues immediately surrounding the bone. This might be due to slippery conditions at the bone/cryogel interface and to a weak link between them when the phantom was built. Because of the poor resolution in the azimuthal direction, this map is also noisy. But it especially demonstrates the interest of considering the 3D motion of soft tissues. The objective function of our algorithm is based on the normalized correlation coefficient, that's why it is also interesting to consider the correlation coefficient map (fig. 2d). Its mean value over the image reaches a satisfying level of 0.93, which means that the estimations can be trusted.

Since the algorithm is three-dimensional, these information (axial strain, lateral and azimuthal displacements) are available for the whole scanned volume. For clinical purpose, the desired parameter could be displayed like a movie (with the z axis corresponding to time), to see its evolution along the azimuth and to provide the physician with a better understanding of the imaged area. We chose here to present the axial strain along the z axis (perpendicular to the US scan) for two different positions (fig. 3). The axial strain for the middle slice (corresponding to the axe of the bone axis) is shown fig. 3a. Here again, the coarse resolution is a limitation. Yet, it is still possible to distinguish the 3 regions. Fig. 3b exhibits the axial strain for an off-centered slice. The bone is not visible at this position, but the healthy and pathological regions can clearly be

differentiated, since the deformation of healthy tissues is approximately twice the deformation of the diseased region.

IV. CONCLUSION

A 3D strain estimator has been described in this paper. Thanks to an optimized adaptive and iterative process, it enables accurate estimations of the axial strain distribution, while considering lateral and azimuthal motion. The strain estimation technique was evaluated on a PVA-cryogel phantom mimicking a pressure ulcer at an early stage. Results are very encouraging, both for the potential of our 3D elastographic method, and for the possibility of detecting this pathology at an early stage. Complementary tests on *in vitro* and *in vivo* biological tissues are now planned.

REFERENCES

- [1] G.T. Nola and L.M. Vistnes, "Differential response of skin and muscle in the experimental production of pressure sores," *Plast. Reconstr. Surg.*, vol. 66, pp. 728-733, Nov. 1980.
- [2] A. Gefen, N. Gefen, E. Linder-Ganz and S.S. Margulies, "In vivo muscle stiffening under bone compression promotes deep pressure sores", *Trans. of the ASME*, vol. 127, pp. 512-524, June 2005.
- [3] J. Ophir, I. Céspedes, H. Ponnekanti, Y. Yazdi and X. Li, "Elastography: a quantitative method for imaging the elasticity of biological tissues", *Ultrasonic Imaging*, vol.13, pp. 111-134, Apr. 1991.
- [4] M. O'Donnell, A.R. Skovoroda, B.M. Shapo and S.Y. Emelianov, "Internal displacement and strain imaging using ultrasonic speckle tracking", *IEEE Trans. Ultrasonics, Ferro. and Freq. Control*, Vol. 41, no. 3, pp. 314-324, May 1994.
- [5] P. Chaturvedi, M.F. Insana and T.J. Hall, "2D Companding for noise reduction in strain imaging", *IEEE Trans. Ultrasonics, Ferro. and Freq. Control*, vol. 45, no. 1, pp. 179-191, Jan. 1998.
- [6] E. Konofagou and J. Ophir, "A new elastographic method for estimation and imaging of lateral displacements, lateral strains, corrected axial strains and Poisson's ratio in tissues", *Ultrasound in Medicine and Biology*, Vol. 24, pp. 1183-1199, Oct. 1998.
- [7] X. Chen, M. J. Zohdy, S. Y. Emilianov and M. O'Donnell, "Lateral Speckle Tracking Using Synthetic Lateral Phase", *IEEE Trans. Ultrasonics, Ferro. and Freq. Control*, vol. 51, no. 5, pp. 540-550, May 2004.
- [8] R. L. Maurice, J. Ohayon, Y. Frétygn, M. Bertrand, G. Soulez and G. Cloutier, "Non-invasive vascular elastography: Theoretical framework", *IEEE Trans. Medical Imaging*, Vol. 23, No 2, pp. 164-180, Feb. 2004.
- [9] E. Brusseau, J. Kybic, J.F. Deprez and O. Basset, "2D locally regularized strain estimation algorithm: Theoretical developments and results on experimental data", *IEEE Trans. Medical Imaging*, to be published, 2007.
- [10] C. Schmitt, G. Soulez, R. L. Maurice, M.F. Giroux, and G. Cloutier, "Non-invasive vascular elastography: toward a complementary characterization tool of atherosclerosis in carotid arteries", *Ultrasound in Medicine and Biology*, to be published, 2007.
- [11] J. Fromageau, J.L. Gennisson, C. Schmitt, R. L. Maurice, R. Mongrain, and G. Cloutier, "Estimation of polyvinyl alcohol cryogel mechanical properties with four ultrasound elastography methods and comparison with gold standard testings", *IEEE Trans. Ultrasonics, Ferro. and Freq. Control*, vol. 54, no. 3, pp. 498-509, Mar. 2007.
- [12] J. Fromageau, E. Brusseau, D. Vray, G. Gimenez, and P. Delachartre, "Characterization of PVA cryogel for intravascular ultrasound elasticity imaging", *IEEE Trans. Ultrasonics, Ferro. and Freq. Control*, vol. 50, no. 10, pp. 1328-1324, Oct. 2003.